

# Time-like Showers Based on Dipole-Antenna Radiation Functions

*R. Frederix*<sup>1</sup>, *W. T. Giele*<sup>2</sup>, *D. A. Kosower*<sup>3</sup>, *P. Z. Skands*<sup>4,2</sup>

<sup>1</sup>CP3, Université catholique de Louvain, 2 Chemin du Cyclotron, B-1348 Louvain-la-Neuve, Belgium

<sup>2</sup>Theoretical Physics, Fermilab MS106, Box 500, Batavia, IL-60510, USA

<sup>3</sup>Service de Physique Théorique, CEA-Saclay, F-91191 Gif-sur-Yvette cedex, France

<sup>4</sup>CERN PH-TH, CH-1211 Geneva 23, Switzerland

## Abstract

We report on the inclusion of massless quarks into the VINCIA time-like shower. Comparisons are made to the dipole-antenna functions used in ARIADNE. At the phenomenological level, we also compare to the PYTHIA 8 shower for hadronic  $Z$  decays at  $\sqrt{s} = m_Z$ , with similar choices for  $\alpha_s$ , the hadronization cutoff, etc.

## 1. INTRODUCTION

In this report we take the next step in the development of the VINCIA shower towards a full-fledged parton shower, embedded into the PYTHIA 8 generator [1, 2]. Previously, we included only the gluonic time-like shower [1]. By including massless quarks we can start making comparisons at LEP energies and make quantitative studies for future linear colliders. As the VINCIA shower is a dipole-antenna shower, we can make direct comparisons with the dipole-antenna functions used in ARIADNE [3].

We also make a phenomenological comparison with the PYTHIA 8 shower. For this purpose, we choose the evolution variable, the hadronization boundary and other parameters in VINCIA as close as possible to the default PYTHIA 8 settings. In this emulation mode we compare a few representative distributions, both infrared safe and infrared regulated observables, such as jet rates, thrust, and parton multiplicities for hadronic  $Z$  decays at  $\sqrt{s} = m_Z$ .

## 2. DIPOLE-ANTENNA FUNCTIONS

The most general form for a leading-log antenna function for massless parton splitting,  $\hat{a}\hat{b} \rightarrow arb$ , can be represented by a double Laurent series in the two branching invariants,

$$a(y_{ar}, y_{rb}; s) = \frac{1}{s} \sum_{\alpha, \beta = -1}^{\infty} C_{\alpha, \beta} y_{ar}^{\alpha} y_{rb}^{\beta}, \quad (1)$$

where

$$s = s_{\hat{a}\hat{b}} = s_{arb} \quad \text{and} \quad y_{ij} = \frac{s_{ij}}{s} \leq 1 \quad (2)$$

are the invariant mass squared of the antenna and the scaled branching invariants, respectively. In principle, eq. (1) could also be multiplied by an overall phase space veto function, restricting the radiation to specific “sectors” of phase space, but we shall here use so-called “global” antenna functions which are summed together without such cuts. Note that we have here written the antenna function stripped of color factors, to emphasize that this part of the discussion is not limited to the leading-color limit.

The coefficient of the most singular term,  $C_{-1, -1}$ , controls the strength of the double (soft) singularity (the “double log” term) and the coefficients  $C_{-1, j \geq 0}$  and  $C_{i \geq 0, -1}$  govern the single (collinear) singularities (“single log” terms). These, in parton shower terminology collectively labeled “leading log” terms, are universal, whereas the polynomial coefficients  $C_{i \geq 0, j \geq 0}$  are arbitrary, corresponding to beyond-leading-log ambiguities in the shower or, equivalently, different NLO subtraction terms in the fixed-order expansion.

	$C_{-1,-1}$	$C_{-1,0}$	$C_{0,-1}$	$C_{-1,1}$	$C_{1,-1}$	$C_{-1,2}$	$C_{2,-1}$	$C_{0,0}$	$C_{1,0}$	$C_{0,1}$
<b>GGG</b>										
$q\bar{q} \rightarrow qq\bar{q}$	2	-2	-2	1	1	0	0	0	0	0
$qg \rightarrow qgg$	2	-2	-2	1	1	0	-1	$\frac{5}{3}$	-1	$\frac{3}{2}$
$gg \rightarrow ggg$	2	-2	-2	1	1	-1	-1	$\frac{5}{3}$	-1	-1
$qg \rightarrow q\bar{q}'q'$	0	0	$\frac{1}{2}$	0	-1	0	1	$-\frac{1}{2}$	1	0
$gg \rightarrow g\bar{q}q$	0	0	$\frac{1}{2}$	0	-1	0	1	-1	1	$\frac{1}{2}$
<b>ARIADNE</b>										
$q\bar{q} \rightarrow qq\bar{q}$	2	-2	-2	1	1	0	0	0	0	0
$qg \rightarrow qgg$	2	-2	-3	1	3	0	-1	0	0	0
$gg \rightarrow ggg$	2	-3	-3	3	3	-1	-1	0	0	0
$qg \rightarrow q\bar{q}'q'$	0	0	$\frac{1}{2}$	0	-1	0	1	-1	1	$\frac{1}{2}$
$gg \rightarrow g\bar{q}q$	0	0	$\frac{1}{2}$	0	-1	0	1	-1	1	$\frac{1}{2}$
<b>ARIADNE2 (re-parameterization of ARIADNE functions à la GGG, for comparison)</b>										
$q\bar{q} \rightarrow qq\bar{q}$	2	-2	-2	1	1	0	0	0	0	0
$qg \rightarrow qgg$	2	-2	-2	1	1	0	-1	-1	0	0
$gg \rightarrow ggg$	2	-2	-2	1	1	-1	-1	$-\frac{4}{3}$	-1	-1

Table 1: Laurent coefficients for massless LL QCD antennae ( $\hat{a}\hat{b} \rightarrow arb$ ). The coefficients with at least one negative index are universal (apart from a re-parameterization ambiguity for gluons). For “GGG” (the defaults in VINCIA), the finite terms correspond to the specific matrix elements considered in [4]. In particular, the  $q\bar{q}$  antenna absorbs the tree-level  $Z \rightarrow qq\bar{q}$  matrix element [5] and the  $gg$  antennae absorb the tree-level  $h^0 \rightarrow gg \rightarrow ggg$  and  $h^0 \rightarrow gg \rightarrow g\bar{q}q$  matrix elements [6]. The  $qg$  antennae are derived from a neutralino decay process [7].

We take the Gehrman-de-Ridder-Glover (“GGG”) antenna functions [4] as our starting point. The corresponding coefficients  $C_{\alpha,\beta}$  for the the five antennae that occur in massless QCD at LL are collected in tab. 1. For reference, we also compare to the radiation functions [8–10] used in the ARIADNE dipole shower [3], which are also the ones used in a recent study by the SHERPA group [11]. Note that the single log terms have a slight ambiguity when gluons are involved, arising from the arbitrary choice of how to decompose the radiation off the gluon into the two antennae it participates in. Nominally, the ARIADNE single log coefficients therefore look different from the GGG ones. However, a re-parameterization of the total gluon radiation, which we label ARIADNE2, reveals that the only real difference lies in the choice of finite terms. Interestingly, while all the ARIADNE radiation functions are positive definite, the equivalent ARIADNE2 one for  $gg \rightarrow ggg$  is not and hence could not be used as a basis for a shower Monte Carlo.

In modern versions of ARIADNE, gluon splitting to quarks has an additional pre-factor  $2/(1 + s_{\hat{a}\hat{b}}/s_{\hat{b}\hat{c}})$ , where  $\hat{c}$  is the neighbor on the other side of the splitting gluon. This is based on comparisons to  $e^+e^- \rightarrow q\bar{q}'q'\bar{q}$  matrix elements and implies that the smaller dipole takes the larger part of the  $g \rightarrow q\bar{q}$  branching. Such effects are not included in VINCIA at this point.

Our convention for color factors is that they count color degrees of freedom. Their normalization should therefore be such that, in the large- $N_C$  limit, they tend to  $N_C$  raised to the power of the number of new color lines created in the splitting. In particular,

$$\begin{aligned} \hat{C}_F &= \frac{N_C^2 - 1}{N_C} = \frac{8}{3}, \\ C_A &= N_C = 3. \end{aligned} \quad (3)$$

For gluon splitting to quarks, the antenna shower explicitly sums over each flavor separately, hence the relevant antenna functions should be normalized to one flavor,  $\hat{T}_R = 1$ . (We use the hatted symbols  $\hat{C}_F$  and  $\hat{T}_R$  to distinguish this normalization from the conventional parton-shower one in which  $C_F = 4/3$  and  $T_R = 1/2$ .)

The complete antenna functions, in the notation of [1, eqs. (2) and (11)], are then

$$\begin{aligned}
A(q\bar{q} \rightarrow qg\bar{q}) &= 4\pi\alpha_s \hat{C}_F a(q\bar{q} \rightarrow qg\bar{q}) , \\
A(qg \rightarrow qgg) &= 4\pi\alpha_s \hat{C}_F a(qg \rightarrow qgg) , \\
A(gg \rightarrow ggg) &= 4\pi\alpha_s N_C a(gg \rightarrow ggg) , \\
A(qg \rightarrow q\bar{q}'q') &= 4\pi\alpha_s a(qg \rightarrow q\bar{q}'q') , \\
A(gg \rightarrow g\bar{q}q) &= 4\pi\alpha_s a(gg \rightarrow g\bar{q}q) ,
\end{aligned} \tag{4}$$

where  $\alpha_s = \alpha_s(\mu_R)$  may depend on the branching kinematics. If so, we use a nominal  $\hat{\alpha}_s = 1$  for generating trial branchings, which are then accepted with probability  $\alpha_s(\mu_R)$  at the point when the full kinematics have been constructed (see below). The possibilities for  $\mu_R$  currently implemented in VINCIA are

$$\mu_R = \begin{cases} \text{type 0} & : K_R 2p_\perp \\ \text{type 1} & : K_R Q_E \\ \text{type 2} & : K_R \sqrt{s_{\hat{a}\hat{b}}} , \end{cases} \tag{5}$$

where  $K_R$  is an arbitrary constant,  $p_\perp$  is defined as in ARIADNE with  $p_\perp^2 = s_{ar} s_{rb} / s_{\hat{a}\hat{b}}$  [3],  $Q_E$  is the evolution variable, and  $\sqrt{s_{\hat{a}\hat{b}}}$  is the invariant mass of the mother dipole-antenna. The default is a 1-loop running five-flavor  $\alpha_s$  with  $\mu_R = p_\perp$  (i.e., Type 0 above, with  $K_R = \frac{1}{2}$ ) and  $\alpha_s(m_Z) = 0.137$  (the default in PYTHIA 8, making comparisons simpler). Alternatively, both fixed and 2-loop running options are available as well [2]. For the pure shower, the dependence on the renormalization scheme of  $\alpha_s$  is beyond the required precision and hence we do not insist on an  $\overline{\text{MS}}$  definition here. Indeed, the default value of  $\alpha_s(m_Z)$  in PYTHIA 8 is determined from tuning to LEP event shapes. Though beyond the scope of the present paper, we note that in the context of higher-order matching, one should settle on a specific scheme, and should then see the dependence on both the scheme and scale choices start to cancel as successive orders are included.

### 3. SHOWER IMPLEMENTATION

Brief descriptions of the VINCIA switches and parameters are contained in the program’s XML “manual”, by default called `Vincia.xml`, which is included together with the code. This file also contains the default values and ranges for all adjustable parameters, which may subsequently be changed by the user in exactly the same way as for a standard PYTHIA 8 run [2].

The default antenna functions are contained in a separate XML file, `Antennae-GGG.xml`. Antennae that are related by charge conjugation to the ones listed tab. 1 are obtained by simple swapping of invariants (e.g.,  $g\bar{q}$  antennae are obtained from the  $qg$  ones). Similarly, antenna functions that are permutations of the ones in tab. 1, such as  $gg \rightarrow \bar{q}qg$ , are obtained by swapping. In view of the probabilistic nature of the shower, all antenna functions are checked for positivity during initialization. If negative regions are found, the constant term  $C_{0,0}$  is increased to offset the difference and a warning is given, stating the new value of  $C_{0,0}$ .

We use the PYTHIA 8 event record [2], which includes Les Houches color tags [12, 13] for representing color connections. At every point during the event evolution, leading-color antennae are spanned between all pairs of (non-decayed) partons for which the color tag of one matches the anti-color tag of the other.

Shower generation proceeds largely as for the pure-gluon case described in [1], including the choice between two evolution variables

$$y_E = \begin{cases} \text{type I (} p_\perp\text{-ordering)} & : y_I^2 = \frac{Q_I^2}{s} = 4 \frac{s_{ar} s_{rb}}{s^2} = 4y_{ar} y_{rb} \\ \text{type II (dipole-mass-ordering)} & : y_{II}^2 = \frac{Q_{II}^2}{s} = 2\min(y_{ar}, y_{rb}) \end{cases} . \tag{6}$$

Note that we do not include an ‘‘angular-ordering’’ option. In conventional parton showers, which use collinear splitting functions, angular ordering gives a good approximation of the coherent dipole radiation patterns we here describe by the antenna functions  $A$ . Since dipole-antenna showers use  $A$  directly, coherence is thus independent of the choice of evolution variable to first order in this formulation (see, e.g., [8]).

For the phase space map an optimal choice for the functional form of the ‘‘recoil angle’’  $\psi_{\hat{a}a}$  (see [1, 3]) away from the soft and collinear limit exists for  $q\bar{q}$  antennae [14]. However, we have not yet implemented this particular subtlety in the VINCIA code. The default choice for all antennae is thus currently the same as for the  $gg \rightarrow ggg$  splitting in ARIADNE [3]

$$\psi_{\text{ARIADNE}} = \frac{E_b^2}{E_a^2 + E_b^2}(\pi - \theta_{ab}), \quad (7)$$

with alternative choices listed in [1].

Trial branchings are generated by numerically solving for  $y_{\text{trial}}$  in the equation  $R = \hat{\Delta}(y_{\text{trial}})$ , where  $R$  is a random number uniformly distributed between zero and one, and the trial Sudakov is [1, eq. (51)]

$$\hat{\Delta}(y_{\text{trial}}) = \exp \left[ - \int_{y_{\text{trial}}}^1 dy_E \int_0^1 dy_{ar} \int_0^{1-y_{ar}} dy_{rb} \delta(y_E - y_E(y_{ar}, y_{rb})) \frac{\hat{A}(y_{ar}, y_{rb})}{16\pi^2} \right], \quad (8)$$

with  $\hat{A}$  an overestimate of the ‘‘true’’ antenna function such that

$$\hat{\mathcal{A}}(y_{ar}, y_{rb}) \equiv s_{arb} \hat{A}(y_{ar}, y_{rb}; s_{arb}, 1) > s_{arb} A(y_{ar}, y_{rb}; s_{arb}, 1) \quad (9)$$

only depends on the rescaled invariants (for instance by using a fixed overestimate of  $\hat{\alpha}_s = 1$  here). Once the full kinematics are known (see below) the trial branching can be vetoed with probability  $1 - A/\hat{A}$ , which by the veto algorithm changes the resulting distribution back to that of  $A$ , as desired.

During program execution, cubic splines of  $\hat{\Delta}$  and  $\hat{\Delta}^{-1}$  are used for the actual trial generation. These splines are constructed on the fly, with the 2-dimensional phase space integrals in eq. (8) carried out either by 2-dimensional adaptive Gaussian quadrature (AGQ) on  $\hat{A}$  directly or (substantially faster) by 1-dimensional AGQ on the primitive function along a contour of fixed  $y_{ar}$ , defined by

$$\begin{aligned} I_a(y_{ar}, y_1, y_2) &= \int_{y_1}^{y_2} dy_{rb} \frac{\hat{A}(y_{ar}, y_{rb})}{16\pi^2} \\ &= \frac{\hat{\alpha}_s C_i}{4\pi} \sum_{\alpha=-1}^{\infty} y_{ar}^{\alpha} \left[ C_{\alpha,-1} \ln \left( \frac{y_2}{y_1} \right) + \sum_{\beta=0}^{\infty} C_{\alpha,\beta} \frac{y_2^{\beta+1} - y_1^{\beta+1}}{\beta+1} \right], \end{aligned} \quad (10)$$

where  $\hat{\alpha}_s$  is the overestimate of  $\alpha_s$  discussed earlier,  $C_i$  represents the color factors appearing in eq. (4), and the phase space limits  $y_{1,2}$  depend on the choice of evolution variable, see below. During initialization, the program checks for consistency between the analytic and numeric integrals and a warning is issued if the numerical precision test fails.

The antenna with the largest trial scale is then selected for further inspection. A  $\phi$  angle distributed uniformly in  $[0, 2\pi]$  is generated, and a complementary phase space invariant,  $z$ , is chosen according to the probability distribution

$$I_z(y_E, z) = \int_{z_{\min}(y_E)}^z dz' |J(y_E, z')| \frac{\hat{A}(y_{ar}, y_{rb})}{16\pi^2}, \quad (11)$$

where  $|J(y_E, z)|$  is the Jacobian arising from translating  $\{y_{ar}, y_{rb}\}$  to  $\{y_E, z\}$  and  $z_{\min}(y_E)$  is the smallest value  $z$  attains inside the physical phase space for a given  $y_E$ . Depending on the type of evolution

variable, as defined in eq. (6), we choose  $\{y_E, z\}(y_{ar}, y_{rb})$  as

$$\begin{aligned} \text{type I} & : y_E = 4y_{ar}y_{rb}, z = y_{rb} \\ & \Rightarrow |J_I| = 1/(4z), z_{\max, \min}(y_E) = \frac{1}{2}(1 \pm \sqrt{1 - y_E}), \end{aligned} \quad (12)$$

$$\begin{aligned} \text{type II} & : y_E = 2y_{ar}, z = y_{rb} \text{ for } z \leq 1 - \frac{1}{2}y_E \\ & y_E = 2y_{rb}, z = y_{ar} + (1 - 2y_{rb}) \text{ for } z > 1 - \frac{1}{2}y_E \\ & \Rightarrow |J_{II}| = 1/2, z_{\min}(y_E) = \frac{1}{2}y_E, z_{\max}(y_E) = 2 - \frac{3}{2}y_E \end{aligned} \quad (13)$$

where, for type II, we have arranged the two separate branches  $y_{ar} < y_{rb}$  and  $y_{rb} < y_{ar}$  one after the other by a trivial parallel displacement in the  $z$  coordinate. Using the Laurent representation of the antenna functions, the analytical forms of  $I_z$  become

$$\text{type I} : \frac{\hat{\alpha}_s C_i}{16\pi} \sum_{\alpha=-1}^{\infty} \left(\frac{y_R}{4}\right)^\alpha \left[ C_{\alpha, \alpha} \ln \frac{z}{z_{\min}(y_E)} + \sum_{\beta \neq \alpha} \frac{z^{\beta-\alpha} - z_{\min}(y_E)^{\beta-\alpha}}{\beta - \alpha} \right] \quad (14)$$

$$\begin{aligned} \text{type II} : & \frac{\hat{\alpha}_s C_i}{8\pi} \left[ I_a \left( \frac{1}{2}y_E, z_{\min}(y_E), \min(z, 1 - z_{\min}(y_E)) \right) \right. \\ & \left. + I_a^T \left( \frac{1}{2}y_E, 1 - z_{\min}(y_E), \max(z, 1 - z_{\min}(y_E)) \right) \right], \end{aligned} \quad (15)$$

where the  $I_a$  is defined in eq. (10) and  $I_a^T$  is the primitive along a direction of fixed  $y_{rb}$

$$I_a^T(y_{rb}, y_1, y_2) = \sum_{\beta=-1}^{\infty} y_{rb}^\beta \left[ C_{-1, \beta} \ln \left( \frac{y_2}{y_1} \right) + \sum_{\alpha=0}^{\infty} C_{\alpha, \beta} \frac{y_2^{\alpha+1} - y_1^{\alpha+1}}{\alpha + 1} \right]. \quad (16)$$

#### 4. NUMERICAL RESULTS

We now turn to a quantitative comparison between PYTHIA 8 and VINCIA for  $e^+e^- \rightarrow Z \rightarrow q\bar{q}$  at  $\sqrt{s} = m_Z$ . We use a 1-loop running  $\alpha_s$  with  $\alpha_s(m_Z) = 0.137$  (the default in PYTHIA 8), with a 5-flavor running matched to 4 and 3 flavors at the  $b$  and  $c$  thresholds, but to eliminate the question of explicit quark mass effects we only allow  $d$  and  $u$  quarks in the  $Z$  decay and subsequent shower evolution. The evolution is terminated at  $p_{\perp \text{had}} = 0.5 \text{ GeV}$ , and we have switched off hadronization so as not to unintentionally obscure the differences between the partonic evolutions. Likewise, photon radiation is switched off in all cases, and in PYTHIA 8 we further switch off gluon polarization effects. For VINCIA, we use three different settings: transverse-momentum ordering with ‘‘GGG’’ antenna functions, dipole-mass ordering with ‘‘GGG’’ antenna functions, and transverse-momentum ordering with the ‘‘ARIADNE’’ antenna functions.

Fig. 1 shows the 3-, 4-, and 5-jet inclusive fractions as functions of the logarithm of Durham  $k_T$ , using the default PYTHIA 8 Durham clustering algorithm [2]. In PYTHIA 8, the 3-jet rate (the set of curves furthest to the right) is matched to the tree-level 3-parton matrix element, whereas the GGG and ARIADNE antenna functions in VINCIA reproduce it by construction. The general agreement on the 3-jet rate is therefore a basic validation of the  $q\bar{q} \rightarrow qg\bar{q}$  antenna implementation. Higher-order effects appear to make the mass-ordered VINCIA slightly softer, which we tentatively conclude is due to this variable favoring soft wide-angle radiation over high- $p_{\perp}$  collinear radiation (as illustrated by fig. 2 in [1]).

Similarly, the 4-jet fractions (the middle set of curves in fig. 1) test the  $gg$  antennae in VINCIA, with the GGG showers here slightly higher and the ARIADNE one slightly lower, in agreement with the differences in  $gg$  antenna finite terms, cf. tab. 1. This trend becomes more pronounced in the 5-jet fraction, since also the  $gg \rightarrow ggg$  function in ARIADNE is softer than GGG.

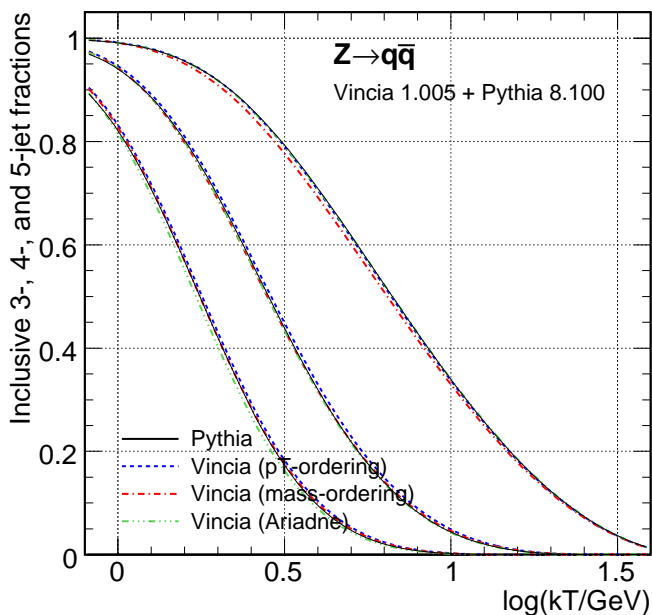


Fig. 1: Inclusive 3-, 4-, and 5-jet fractions.

We may now study further distributions, as a representative example of which we take thrust, illustrated as  $1 - T$  in the top row of fig. 2. The full distribution is shown to the left with a closeup of the region  $1 - T < 0.1$  to the right. The region  $0.1 < 1 - T < \frac{1}{3}$  is dominated by well-separated three-jet configurations. In the tail,  $1 - T > \frac{1}{3}$ , a matching to  $e^+e^- \rightarrow 4$  jets would be required to improve the accuracy. In the region below  $1 - T = 0.1$ , however, this would not help. These are three-jet configurations which are “nearly two-jet”. Here, the type and size of the Sudakov suppression is essential, the first fixed order of which could be accessed by 1-loop matching, but since the fixed-order expansion is poorly convergent in this region anyway, the disagreement is more likely to be cured by a systematic inclusion of higher-logarithmic effects in the showers (either implicitly, by “clever choices” of evolution, renormalization, and kinematic variables in the LL shower, or explicitly, by a systematic inclusion of NLL splittings). It should be noted, however, that hadronization and hadron decay effects are important in the region below

$$1 - T \sim 1 - \max(x_k) = \min(y_{ij}) \lesssim \frac{(\text{A few GeV})^2}{m_Z^2} \lesssim 0.01, \quad (17)$$

where the  $x$  and  $y$  fractions pertain to 3-jet configurations. This complicates the separation of genuine non-trivial higher-log effects from non-perturbative effects when comparing to experimental data at currently accessible collider energies.

Finally, as illustration of an infrared sensitive quantity, in the bottom row of fig. 2 we plot the probability distribution of the number of partons produced at the shower termination for each of the four models. The total number of partons is shown to the left and the number of quarks (not counting anti-quarks) to the right. The definitions of  $p_\perp$  in PYTHIA and in VINCIA/ARIADNE, respectively, are not exactly identical, but they have the same infrared limiting behavior [15], and hence a comparison of the number of resolved partons with a cutoff at  $p_{\perp\text{had}} = 0.5 \text{ GeV}$  should be meaningful. Since we have also chosen the same  $\alpha_s$  values etc., the basic agreement between the models in the lower left-hand plot in fig. 2 reconfirms that there are no large differences between the showers, even at the infrared sensitive level. ARIADNE produces somewhat fewer partons, consistent with the ARIADNE radiation functions being slightly softer. On the right-hand plot, however, it is interesting to note the first substantial difference between PYTHIA 8 and the VINCIA showers. The PYTHIA shower produces

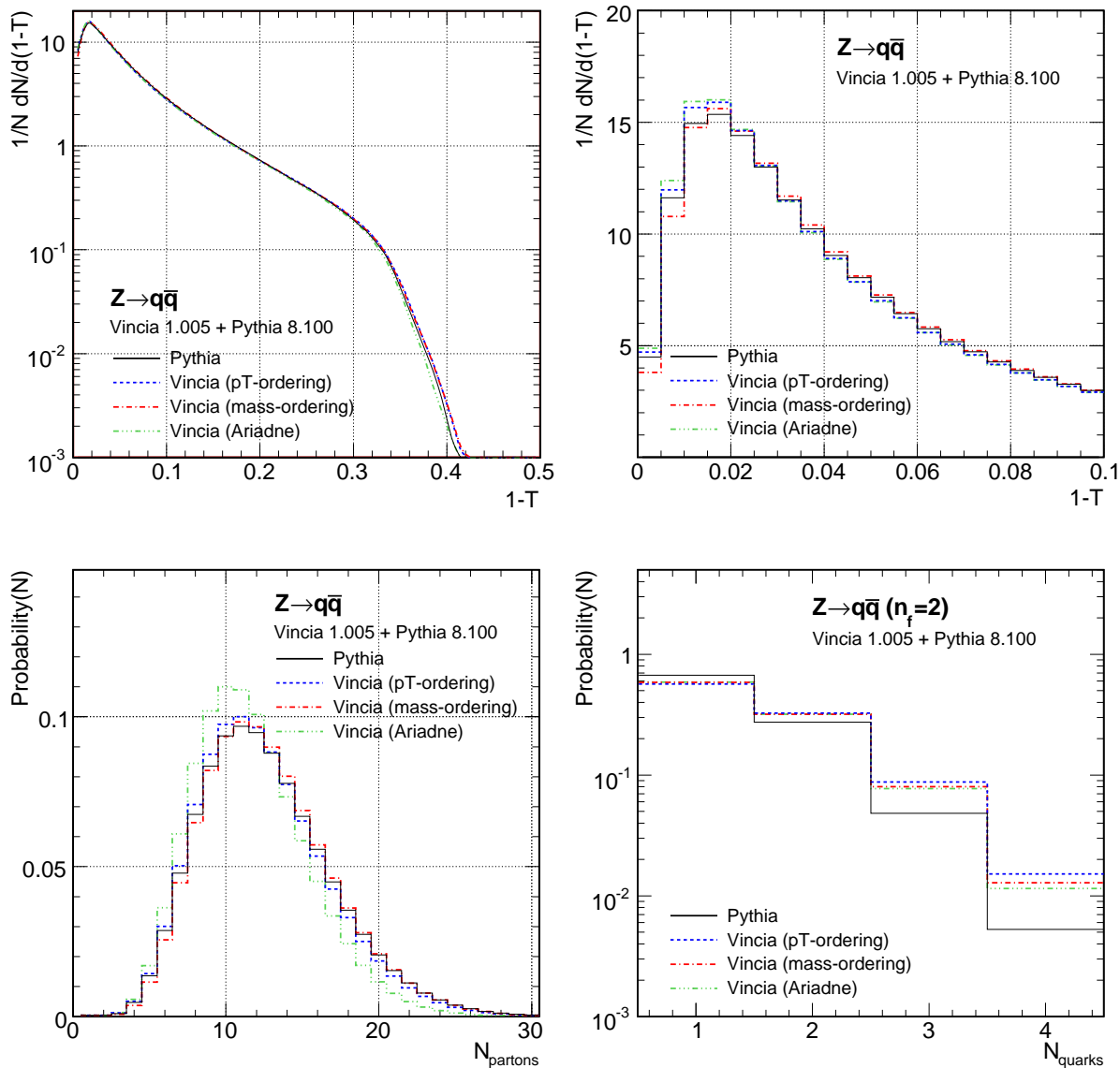


Fig. 2: Top row: Thrust,  $1 - T$ . Bottom row: Number of partons (left) and number of quarks (right) at shower termination, with 2 massless quark flavors.

significantly fewer quarks than any of the VINCIA showers, despite its being higher or comparable on the total number of partons (cf. the left-hand plot). A similar difference between parton and dipole-antenna showers was observed in an earlier ARIADNE study [10], in which a comparison was made to the virtuality-ordering of traditional parton showers. It is interesting that we here observe the same trend when comparing to the PYTHIA 8 shower which is ordered in  $p_{\perp}$ . Finally, we note that this difference will also have practical consequences; in the context of tuning of hadronization models, the VINCIA showers will presumably need a stronger suppression of non-perturbative strangeness production to make up for the larger perturbative production rate, as compared to PYTHIA 8.

## CONCLUSIONS

We have presented the inclusion of massless quarks into the VINCIA shower algorithm, implemented as a plug-in to the PYTHIA 8 event generator. The dipole-antenna radiation functions are expressed as double Laurent series in the branching invariants, with user-specifiable coefficients. At the analytical level, we compare the coefficients of the ‘‘GGG’’ antenna functions [4] used by default in VINCIA to

the ARIADNE ones [3]. Modulo a re-parameterization of emissions from gluons, we find the double and single log coefficients to be identical, as expected. The finite terms, however, are generally somewhat smaller for the ARIADNE functions. This represents a genuine shower ambiguity which can only be systematically addressed by matching to fixed-order matrix elements.

At the phenomenological level, we have also compared to the hybrid parton-dipole shower in PYTHIA 8 [2] for  $e^+e^- \rightarrow Z \rightarrow q\bar{q}$  at  $\sqrt{s} = m_Z$ . We find a good overall agreement, even at the level of an infrared sensitive quantity such as the final number of partons. For the number of quarks produced, however, PYTHIA 8 is markedly lower than any of the VINCIA showers we have compared to here.

## ACKNOWLEDGMENTS

We thank J. Andersen, Y. Dokshitzer, G. Marchesini, Z. Nagy, T. Sjöstrand, D. Soper, and G. Zanderighi for enlightening discussions. DAK is supported in part by the Agence Nationale de la Recherche of France under grant ANR-05-BLAN-0073-01. This work has been partially supported by Fermi Research Alliance, LLC, under Contract No. DE-AC02-07CH11359 with the United States Department of Energy.

## References

- [1] W. T. Giele, D. A. Kosower, and P. Z. Skands, [arXiv:0707.3652 \[hep-ph\]](#).
- [2] T. Sjöstrand, S. Mrenna, and P. Skands, [arXiv:0710.3820 \[hep-ph\]](#).
- [3] L. Lönnblad, *Comput. Phys. Commun.* **71** (1992) 15–31.
- [4] A. Gehrmann-De Ridder, T. Gehrmann, and E. W. N. Glover, *JHEP* **09** (2005) 056, [[hep-ph/0505111](#)].
- [5] A. Gehrmann-De Ridder, T. Gehrmann, and E. W. N. Glover, *Nucl. Phys.* **B691** (2004) 195–222, [[hep-ph/0403057](#)].
- [6] A. Gehrmann-De Ridder, T. Gehrmann, and E. W. N. Glover, *Phys. Lett.* **B612** (2005) 49–60, [[hep-ph/0502110](#)].
- [7] A. Gehrmann-De Ridder, T. Gehrmann, and E. W. N. Glover, *Phys. Lett.* **B612** (2005) 36–48, [[hep-ph/0501291](#)].
- [8] G. Gustafson, *Phys. Lett.* **B175** (1986) 453.
- [9] G. Gustafson and U. Pettersson, *Nucl. Phys.* **B306** (1988) 746.
- [10] B. Andersson, G. Gustafson, and L. Lönnblad, *Nucl. Phys.* **B339** (1990) 393–406.
- [11] J.-C. Winter and F. Krauss, [arXiv:0712.3913 \[hep-ph\]](#).
- [12] E. Boos *et. al.*, [hep-ph/0109068](#).
- [13] J. Alwall *et. al.*, *Comput. Phys. Commun.* **176** (2007) 300–304, [[hep-ph/0609017](#)].
- [14] R. Kleiss, *Phys. Lett.* **B180** (1986) 400.
- [15] T. Sjöstrand and P. Z. Skands, *Eur. Phys. J.* **C39** (2005) 129–154, [[hep-ph/0408302](#)].